J. Astron. Space Sci. 19(3), 173–180 (2002)

HALO EMISSION OF THE CAT'S EYE NEBULA, NGC 6543: SHOCK EXCITATION BY FAST STELLAR WINDS

Siek Hyung[1†] and Seong-Jae Lee[2]

[1]School of Science Education (Astronomy), Chungbuk National University, 48 Gaeshin-dong Heungduk-gu, CheongJu 361-763, Korea

[2]Dept. of Astronomy and Space Science, Chungnam National University, 220 Kung-dong, Yusong-gu, Daejon 305-764, Korea

E-mail: hyung@trut.chungbuk.ac.kr, seong@canopus.chungnam.ac.kr

(Received June 24, 2002; Accepted August 2, 2002)

ABSTRACT

Images taken with the Chandra X-ray telescope have for the the first time revealed the central, wind-driven, hot bubble (Chu et al. 2001), while Hubble Space Telescope (HST) WFPC2 images of the Cat's Eye nebula, NGC 6543, show that the temperature of the halo region of angular radius $\sim 20''$, is much higher than that of the inner bright H II region. With the coupling of a photoionization calculation to a hydrodynamic simulation, we predict the observed [O III] line intensities of the halo region with the same O abundance as in the core H II region: oxygen abundance gradient does not appear to exist in the NGC 6543 inner halo. An interaction between a (leaky) fast stellar wind and halo gas may cause the higher excitation temperatures in the halo region and the inner hot bubble region observed with the Chandra X-ray telescope.

Keywords: stellar wind, gas-dynamics, planetary nebulae, individual (NGC 6543)

1. INTRODUCTION

Planetary Nebulae (PNe) are ejecta from the highly evolved stars which have reached the end of their life as thermonuclear burning sources. PNe are believed to go through three phases of mass loss: 1) 'Red Giant Wind' phase, $\dot{M}\sim 10^{-7}$ $M_\odot$ yr^{-1}, 2) 'Superwind' phase, $\dot{M} \sim 10^{-5}$ $M_\odot$ yr^{-1}, and 3) an ionized fast stellar wind phase from the hot central star of the PN (CSPN), $V \sim 10^3$ km s^{-1}, $\dot{M} \sim 10^{-8}$ $M_\odot$ yr^{-1}. The faint outer parts of evolved PNe often show distinctly different morphological forms. For example, the giant spherical outer halos around NGC 6852 and NGC 6543 have filamentary blobs, and emit the high-excitation [O III] lines. These blobs or filamentaries show very strong [O III] emission. Comparison of the halo and bright core nebular gas indicates that the halo emission of these two PNe is thermal, and not reflected (Middlemass et al. 1989). On the other hand, faint, broad [O III] 5007 line profiles found in the NGC 3242 halo appear to indicate scattered light (Meaburn et al. 2000). These diffuse and bright halo blobs trace

†corresponding author

the outflows that preceded the PN evolutionary phase. Theoretically, most PNe are expected to have such diffuse regions due to the preceding evolutionary phases.

Many PNe may harbor very high temperature inner regions: recent Chandra observations detected X-ray emission in the central core H II region, not only from well-known X-ray sources like NGC 6543, but also from typical PNe, such as BD +30 3639 and NGC 7027. However, it is almost impossible to find such evidence from optical spectra. One may obtain some clues from the spectroscopic data analysis. For example, Middlemass et al. (1989) derived the halo [O III] electron temperatures, T_e = 14 700 K and 10 000 K, in the giant haloes of NGC 6543 and NGC 6826, respectively, which is about 3000 – 5000 K higher than in the inner H II nebular region. These halo regions are known to be kinematically inert, i.e. velocities limited to less than a few km s^{-1}.

For an explanation of the high electron temperatures in the giant haloes (with angular radius of a few arc-minutes), Bryce et al. (1992) suggested a bow shock scheme with moderate interacting winds, i.e. a 20 km s^{-1} wind (Mach number = 2.2) driving into a 5 km s^{-1} wind: for an assumed temperature of 8800 K in the flow, the post-shock temperature would be 1.7 times the pre-shock temperature, i.e. ~15 000 K. This moderate bow shock scheme had not yet been tested with a detailed simulation. Recently, Hyung et al. (2001) investigated a similar slow wind interaction scheme, to accommodate the high electron temperature in the inner haloes of NGC 6543 (on a scale of a few 10 arcseconds): the main objective of their study was, however, to explain the multiple shell or ring formation in the inner halo, confirmed by Balick et al. (2001). A time-varying slow wind from the CSPN, changing sinusoidally from 40 to 80 km s^{-1} with a period of e.g. 200 years, may be responsible for multiple halo rings. This slow interaction scheme, however, cannot accommodate the much higher Chandra X-ray temperatures of the core H II inside the halo. By contrast, in this investigation, we investigate the shock heating caused by an interaction of a mass-loaded fast stellar wind against an out-going slowly expanding gas phase.

2. OBSERVATIONS

Many spectroscopic investigations were carried out on NGC 6543, but these studies were focused mainly on the bright core H II region. NGC 6543 has an extended outer halo that consists of the remnants of the original giant star atmosphere. We analyzed the Hubble Space Telescope (HST) WFPC2 [O III] images of NGC 6543, and derived the electron temperature map for the core H II region and halo region. The HST WFPC2 archive images were taken from the HST archive data center. Although two [O III] 4363 & 5007 HST images would give us an electron temperature information in [O III] emitting zones. we also needed Hα or Hβ images to eliminate the continuum contribution from the above [O III] images. Hence, we used 3 best WFPC2 archive images, i.e., U27Q0103T ([O III] 4363); U27Q010FT(Hα); and U27Q010AT ([O III] 5007), which were all secured on September 18, 1994 UT to investigate the X-ray emission characteristics of NGC 6543. The exposure times are 1200, 200 and 600 seconds, respectively. Detailed reduction method has been described in Hyung et al. (2001). In Fig. 1, we present the electron temperature distribution along the major axis at PA = $-32°$ (summed over 3 pixels, corresponding to the slit width ~ $0.3''$). The central part, showing an electron temperature over 15 000 K, is in fact caused by an observational error, due to pixel bleeding from the saturated central star in the [O III] 4363 image. One can see a number of peaked clumps with FWHM ~ $0.3'' - 0.4''$, where the electron temperature increases sharply. These may be blobs

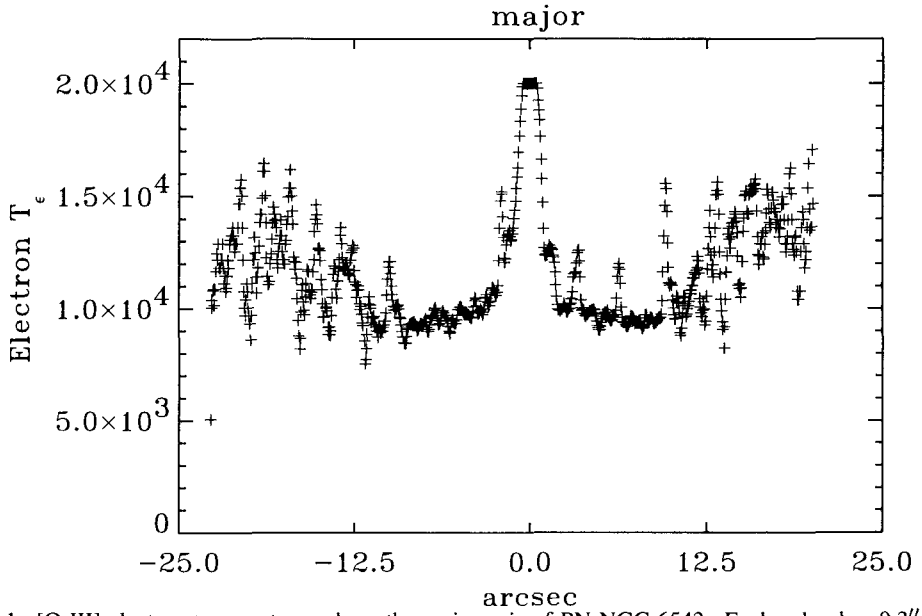

Figure 1. [O III] electron temperatures along the major axis of PN NGC 6543. Each value has 0.3″ spatial resolution. The core H II region is within the angular radius ~ 12″, while the inner halo is outside of the core. The upper limit of electron temperature was artificially set in this plot at 20 000 K, for the region near the CSPN.

or filamentaries. The electron temperatures of the outer haloes are higher than those of the main ionized nebular shells. Hyung et al. (2001) already discussed the characteristics of halo blobs (or the numerous rings defined by Balick et al. 2001). The maximum electron temperature in the halo occurs at a radial distance of r ~ 18″ (~0.09pc for an assumed distance of 1 kpc), beyond which it drops again.

3. SHOCK EXCITATION BY FAST WIND

Chandra X-ray image shows that a hot bubble actually exists in this object, and that it is located in the core H II region (Chu et al. 2001). Thus, a hydrodynamic simulation should produce both the hot bubble core and the high electron temperatures indicated by the HST images. Hyung et al. (2000) and Middlemass et al. (1989) already confirmed that the photoionization model related to the CSPN UV photons is not responsible for the rise of T_e in the outer part of the photoionized PN.

3.1 Description of the method

The majority of published numerical hydrodynamic models concentrate on a shaping scenario for the main core nebula. Our goal, on the other hand, is to reproduce the higher halo temperatures. Here we explore a simple case in which the energy of the fast wind of the CSPN has somehow leaked out into the halo. With the numerical simulation, our objective is to reproduce the observed line intensities and physical conditions in the halo, i.e. electron density, electron temperature, and flow speed.

Table 1. Input parameters for the simulation.

Distance	1000 pc
$\dot{M}_{slow}$	10^{-6} $M_\odot$ yr^{-1}
(ρ_{slow} at 0.01pc	7.48×10^{-21} g cm^{-3})
V_r(slow)	5 km s^{-1}
$\dot{M}_{fast}$	10^{-7} $M_\odot$ yr^{-1}
(ρ_{fast} at 0.01pc	1.87×10^{-24} g cm^{-3})
V_r(fast)	2000 km s^{-1}
d_{in}(boundary)	0.01 pc
d_{out}(boundary)	0.15 pc (30″)
Central Star $T_\star^1$	48 000 K (log g = 6.90)
Central Star L($\star$)[1]	3510 $L_\odot$

[1]: Improved Sobolev approximation (ISA) model atmosphere with He/H = 60 (see Hyung et al. 2000 and references therein).

The hydrodynamic part of the code is based on Roe's approximate Riemann solver (Mellema 1993, Eulderink & Mellema 1995). In each numerical time step, the heating and cooling rates are calculated using the photoionization code from Hyung et al. (2000). Since we are not concerned here with the shaping of the nebula, and a two–dimensional hydrodynamic simulation with an exact photoionization treatment would be much too time consuming, we consider the one-dimensional (spherical) case. Because we are investigating the shock-heated region, or clumps, we must resolve the cooling region behind the shock front, and use non-equilibrium values for the temperatures and heating and cooling rates. The photoionization code was modified to provide the appropriate heating and cooling rates, and the temperature was updated using these rates. To resolve the cooling region, we used 1000 computational cells of size 1.4×10^{-4} pc. At this cell size, the cooling time is also longer than the standard hydrodynamic time step set by the Courant-Lewis-Friedrichs (CFL) condition.

We assumed the slow wind speed to be 5 km s^{-1}. The observed electron density of the halo region, obtained from the [O II] diagnostics, can set a constraint for the mass loss rate for the slow wind. Middlemass et al. (1989) found 35^{+100}_{-35} cm^{-3} (in the halo region outside the HST image). Taking a (pre–shock) number density of $n_H \simeq 20$ cm^{-3} at 0.15 pc, we arrive at a mass loss rate for the slow wind of $\dot{M}_{slow} = 10^{-6}$ $M_\odot$ yr^{-1}. Using non-LTE model atmospheres, several authors have fitted the P Cygni profiles observed in IUE spectral region, to derive terminal velocities for the CSPN wind: 2150 km s^{-1} (Castor et al. 1981), 1900 km s^{-1} (Bianchi et al. 1986, Perinotto et al. 1989), and 1600 km s^{-1} (de Koter et al. 1996). For the CSPN mass loss rate, the above analyses yield values ranging from 0.4×10^{-7} to $\sim3.2\times10^{-7} M_\odot$ yr^{-1}. In our simulation, we take the fast wind speed to be 2000 km s^{-1}, and its mass loss rate $\dot{M}_{fast} = 10^{-7}$ $M_\odot$ yr^{-1}. We assume it to be constant in time. We assume the fast wind is a 'leaky' stellar wind bubble: if the material of the fast wind is

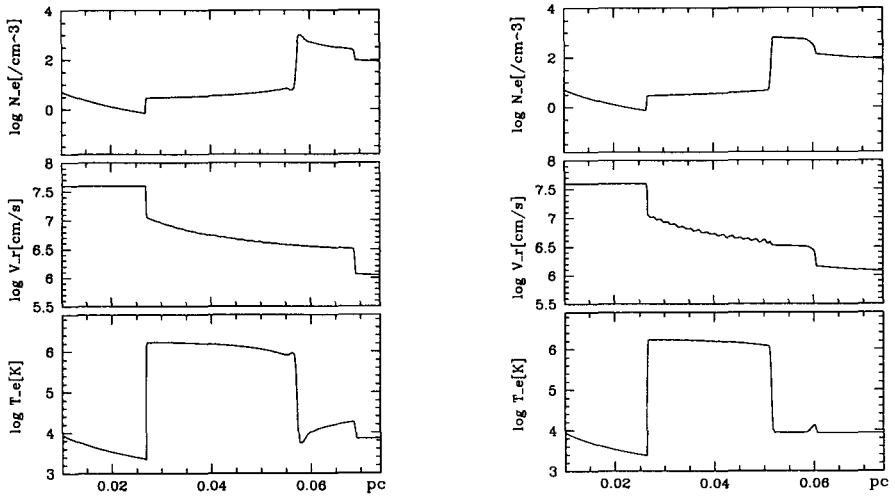

Figure 2. Hydrodynamical simulation result – electron density, velocity, and electron temperature. (a) non-radiative model result at t = 1000 years. (b) radiative model result at t = 1500 years.

quite clumpy, a mass loaded flow will proceed beyond the core nebula into the halo region. For the CSPN spectral energy distribution, we adopt the hardened or 'broken–out' UV given by Hyung et al. (2000). At the start of a simulation, the initial value of the electron temperature is given by the equilibrium temperature provided by photoionization model. For the abundances we used the values derived by Hyung et al. (2000) for the core nebula: He/H = 0.13, C/H = 5.0(-5), N/H = 1.2(-4), O/H = 3.0(-4), Ne/H = 5.0(-5), S/H = 7.0(-6), Ar/H = 4.0(-6), Cl/H = 1.0(-7), K/H = 1.5(-8), and Si/H = 2.2(-6). Other parameters adopted in the simulations are listed in Table 1. The main concern here is to know whether we need to enhance the above oxygen abundance to fit the [O III] line intensities of the halo region.

3.2 Results of the simulation

Firstly, in Fig. 2(a), we show the density, velocity, and temperature at t = 1000 years, for a simulation in which the photoionization code was not used (non–radiative or adiabatic case). As is well known from previous analytical and numerical work (*e.g.* Mellema 1993), four regions develop: 1) unshocked fast wind ($\sim$ 0.03 pc); 2) shocked fast wind or hot bubble (0.03 $\sim$ 0.09pc); 3) shocked slow wind or swept-up shell (0.09 pc $\sim$ 0.107pc); 4) unshocked show wind (>0.107 pc).

Figure 2(b) shows the result of a radiative model at an evolutionary time of t = 1500 years. In this case, the energy losses through cooling have been substantial enough to reduce the expansion velocity of the outer shock. In order to compare our simulation to the HST result in Fig. 1, we needed to reproduce a possible such boundary, and therefore we continued the simulation till t = 1500 years, at which point the outer shock is located at $r \sim 0.12$ pc. One sees how the cooling behind the outer shock has led to higher densities, and also a smaller extent of the region between the outer shock and the contact discontinuity.

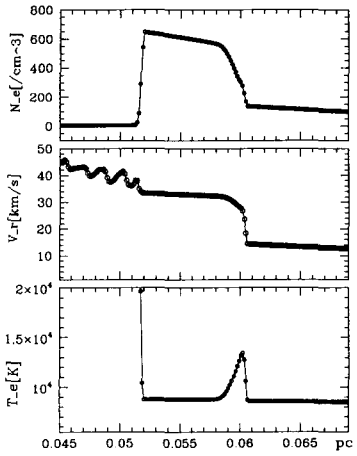

Figure 3. Physical conditions near the shock front.

The inner region is mostly very low in density. The physical condition which has the dominant effect on the nebular emission is, in fact, the high density region near the shock boundary, i.e. 0.115 pc $<$ r $<$ 0.128 pc. Thus, in Fig. 3, we present a detailed result of the region near the shock boundary. We see the cooling region behind the shock: the electron temperature falls from ~80 000 K to about 9000 K (in the non-radiative case, the post–shock temperature is 10^5 K). The electron density across the shock and cooling region goes up from ~40 cm^{-3} to 800 cm^{-3}, a compression by a factor 20. The velocity of the post–shock gas is around 80 km s^{-1}, which is inconsistent with the observations, unless we are only observing small tangential velocities.

Since our hydrodynamic calculation also includes an exact photoionization model, we are able to compare it with the observations for I(5007)/I(4363), and the derived T_e. Obviously, it is mainly the high density thin shell region between 0.117 pc and 0.125 pc which contributes to the intensities. Table 2 lists the results. The 2nd column gives the line intensities obtained from the HST images (see Fig. 1 of Hyung et al. 2001), while the 2nd and 3rd columns list the predictions from our simulations. The simulations give I(5007) / I(4363) $\simeq$ 70, and T_e ([O III]) $\simeq$ 13 500 K. These values are close to the HST results (i.e. to the peak temperatures in the halo). The photoionization also predicts the excitation temperature for other ions, e.g. T_e (H recombination) $\sim$ 12 500 K, a value lower than found using the [O III] lines. A similar effect is seen in the observations, although with a larger amplitude (see Middlemass et al. 1989). Middlemass et al. observed that an abundance difference could cause the peculiar intensities of the [O III] line emission in the halo. Note that the abundance values adopted from the core H II region fitted the halo [O III] line intensities and ratios within the observational errors. This agreement suggests that a spatial gradient in oxygen abundance does not exist, contrary to the result by Middlemass et al.

4. DISCUSSION

We introduced a relatively simple interacting wind scheme, between fast and slow winds, to fit the halo emission line intensities and high electron temperatures of the NGC 6543 halo region, with-

Table 2. Shock excited emission from the NGC 6543 halo.

	HST Intensity	1000yr[a]	1500yr[b]
[O III] 4363	10 – 40	18.61	19.67
4959	—	459.3	471.1
5007	500 – 1200	1323	1357
I(5007)/I(4363)	140 – 33 (70[c])	71.1	70.0
T_e([O III]) (K)	13 500[c]	13 400	13 600
T_e(Hα) (K)	—	12 300	12 800

All intensities are given based on the scale of I(Hβ) = 100.0 and line intensities in the 2nd column from Hyung et al. (2001). [a]: the prediction at t = 1000 years (for the shocked slow wind zone between 0.07 pc and 0.085 pc); [b]: the prediction at t = 1500 years (for the shocked slow wind zone between 0.115 pc and 0.13 pc). See text and Fig. 3; [c]: line ratio for the high electron temperature halo (see Fig. 1).

out introducing oxygen abundance anomaly. The thermal properties of the gas in the halo are set by photoionization heating, and also possibly by shock heating. Thus, our predictions are based on gas-dynamical studies, via the coupling of a hydrodynamic simulation to a photoionization calculation. In our investigation, we adopted a slow wind with a mass loss rate similar to the slow wind phase of a PN precursor star at the tip of the Asymptotic Giant Branch, i.e. 10^{-7} and 10^{-5} $M_\odot$ yr^{-1}, with velocities around 5 km s^{-1} (Pottasch 1984); while the fast wind speed of 2000 km s^{-1} was adopted for the current central WR star. This simulation produced a shock front of rather fast $\sim$80 km s^{-1}. Note that the apparently extreme shock conditions (T_e = 10 000 $\sim$ 80 000 K; see Fig. 3) in fact produced [O III] line intensities of much lower electron temperature $T_e \simeq$ 13 500 K (see Table 2). Reproducing the high [O III] electron temperatures in the halo appeared to be simple. However, the simultaneous prediction of the correct line intensities would be very difficult. We were nevertheless successful in obtaining the high electron temperatures and line intensities in the halo region.

Multiple halo ring structures which had been confirmed by Balick et al. (2001), were successfully simulated by an alternative slow wind scheme (Hyung et al. 2001). However, this alternative slow scheme has also its own limitation, e.g. perhaps not suitable for an explanation of the inner hot bubble zone: the recent Chandra result (Chu et al. 2001) shows the X-rays come only from the inner core of an elongated core H II region (closed shell?). Our simulation also has its own limit: it does not represent the whole halo emission zone, but it only produces a small region (or a mainly empty thin shell). Our analysis indicated that a mass loaded fast wind with 10^{-7} $M_\odot$ yr^{-1} would not produce any meaningful optical or X-ray emission (or hot bubble) in the shocked fast wind region, because of a too low density in this region. To predict any meaningful hot bubble core H II region or inside the inner halo, the mass loss rate must be at least one or two orders higher. Detailed simulation for this elongated core X-ray image is beyond our current computational limits. As mentioned in Section 2, the central parts of the WFPC2 [O III] 4363 image are strongly affected by bleeding from the bright CSPN. Thus, it produces a falsely higher electron temperature >15 000 K at the center (see Fig. 1). However, there appears to be a sign of another shock phenomenon in the CSPN neighborhood, i.e. at angular distance $\sim 2-3''$ from the center, caused by another wind interaction. If one

wants to solve the shaping and emission mechanism for the whole PN, i.e. the CSPN neighborhood, the core H II, and the currently studied inner $\sim 20''$ and outer $\sim 50'$ giant haloes, it would require a longer hydrodynamic time scale (and a long CPU time), which is beyond the computational scope of the current study. For such detailed investigations, one must also secure various monochromatic images of other diagnostic lines, e.g. [S II] and [N II]. These observations would certainly provide necessary constraints on such a future trial.

High-excitation, giant, and outer filamentary blobs, similar to those of NGC 6543, have been recently discovered in the outer region of the apparently normal PN NGC 7009 (Moreno-Corral et al. 1998). Many PNe, such as NGC 2392 (Eskimo nebula), NGC 2346 (Hourglass nebula), and NGC 3242 (Ghost of Jupiter), are known to have bright blobs in the halo, or in the outer shells, as revealed by recent HST observations, or through adaptive optics imaging with large ground-based telescopes. These halo emission line characteristics and the Chandra X-ray hot bubbles may be related to the same basic heating mechanism. In conclusion, a fast stellar wind and resulting shock excitation appear to be involved with the higher electron temperatures in the halo of NGC 6543. Based on our result, we also conclude the oxygen abundance gradient does not exist in the NGC 6543 inner halo.

ACKNOWLEDGMENTS: This research was supported by the Grant KOSEF R01-1999-000-00022 0 and by the Grant KRF 2000-015-DP0445. We are thankful to the KISTI staff for their permission to use GS320 Supercomputer (The 3rd Supercomputing Application Support Program). SH is also thankful to Dr. Garrelt Mellema for supplying his Roe-solver hydrodynamic code.

REFERENCES

Balick, B., Wilson, J., & Hajian, A. R. 2001, AJ, 121, 354
Bianchi, L., Cerrato, S., & Grewing, M. 1986, A&A, 169, 277
Bryce, M., Meaburn, J., Walsh, J. R., & Clegg, R. E. S. 1992, MNRAS, 254, 477
Castor, J. I., Lutz, J. H., & Seaton, M. J. 1981, MNRAS, 194, 547
Chu, Y. H., Guerrero, M. A., Gruendl, R. A., Williams, R. M., & Kaler, J. B. 2001, ApJ, 553, 69
de Koter, A., Heap, S. R., & Lanz, T. 1996, Hydrogen deficient stars, ASP Conference 96, eds. C. S. Jeffery & U. Heber (ASP: San Francisco), 141
Eulderink, F., & Mellema, G. 1995, A&AS, 110, 587
Hyung, S., Aller, L. H., Feibelman, W. A., Lee, W. B., & de Koter, A. 2000, MNRAS, 318, 7
Hyung, S., Mellema, G., Lee, S.-J., & Kim, H. 2001, A&A, 378, 587
Meaburn, J., O'Connor, J. A., Lopez, J. A., Bryce, M., Redman, M. P., & Noriega-Crespo, A. 2000, MNRAS, 318, 561
Mellema, G. 1993, Ph.D thesis, Leiden University
Middlemass, D., Clegg, R. E. S., & Walsh, J. R. 1989, MNRAS, 239, 1
Moreno-Corral, M., de La Fuente, E., & Gutierrez, F. 1998, RMxAA, 34, 117
Perinotto, M., Cerruti-Sola, M., & Lamers, H. J. G. L. M. 1989, ApJ, 337, 382
Pottasch, S. R. 1984, Planetary nebulae (Dordrecht: Reidel), p.248